

The Electron Falls Apart

There are two kinds of physics; one is to search for elements in nature and the other is to examine the diversity of nature. The condensed matter physics which our group is working on is in the latter. An electron is an elementary particle. However, when many of them interact strongly in materials, they give rise to a variety of quantum phenomena. In addition, electrons cannot often keep their own properties in such correlated states.

Spin and charge are inseparable traits of an electron, but in one-dimensional solids, their separation into collective modes-as independent excitation quanta (or particles) called spinons and holons is expected.

We have identified, for the first time, both theoretically and experimentally, the evidence of spin-charge separation, i.e., in the angle-resolved photoemission (ARPES) spectrum in SrCuO₂ the single quasiparticle peak splits into a spinon-holon two peak structure.

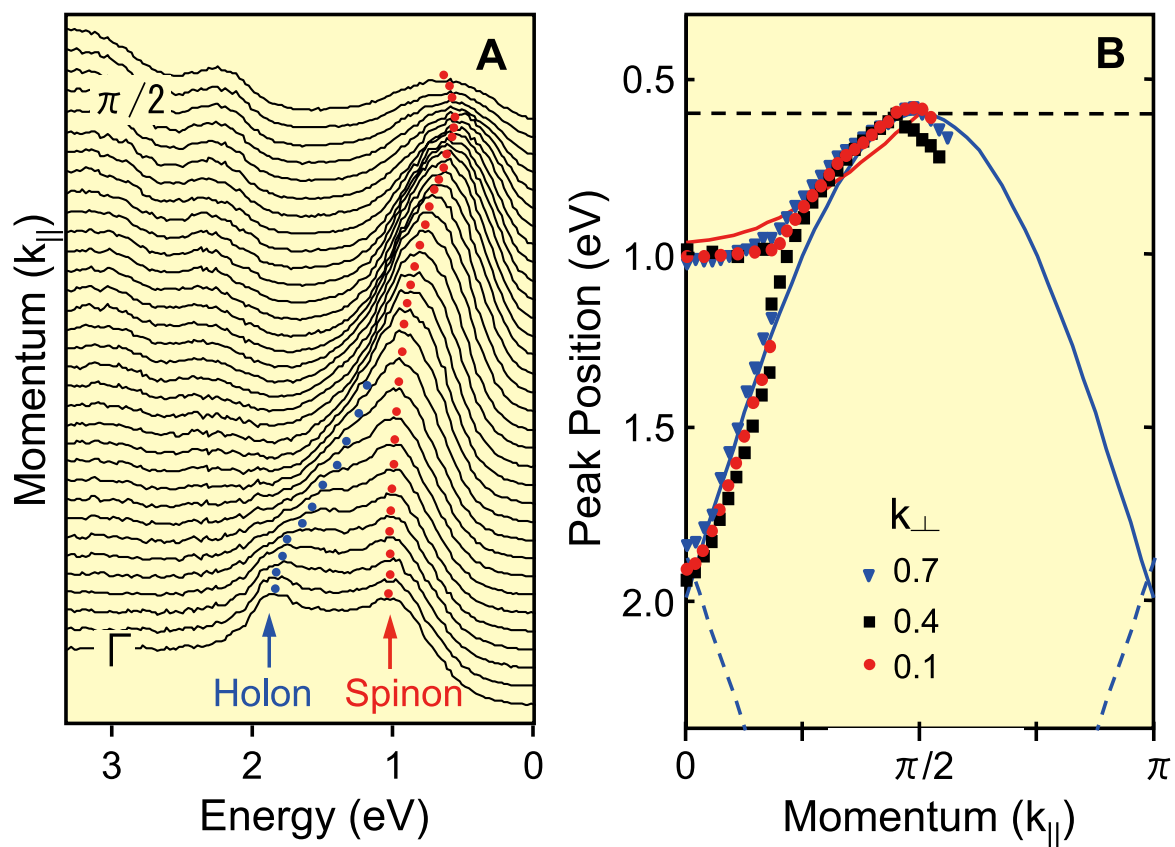


Fig.1. (a) The angle-resolved photoemission spectrum in SrCuO₂. (b) The experimental and theoretical (Solid and dashed lines) dispersions of spinon and holon.

References

[1] B.J.Kim, H. Koh, E. Rotenberg, S.-J.Oh, H. Eisaki, N. Motoyama, S. Uchida, T. Tohyama, S. Maekawa, Z.-X. Shen and C. Kim, Nature Physics 2, 397 (2006).

Contact to

Sadamichi Maekawa (Theory of Solid State Physics Division)
e-mail: maekawa@imr.tohoku.ac.jp

High Magnetic Field X-ray Spectroscopy on YbInCu₄ -a New Tool of Valence State in Intermetallics-

The world strongest and smallest magnet has been developed for high field X-ray spectroscopy. The first experiment is made for the valence state transition of YbInCu₄ and a field variation of the valence is clearly determined. The system opens a new way to investigate the valence state of intermetallics in very high magnetic fields.

A synchrotron X-ray is a powerful tool to investigate materials for the extremely strong intensity and the tunability in X-ray regime. This can be applied not only for a structure analysis but also for X-ray spectroscopy such as X-ray absorption (XAS) and magnetic circular dichroism (MCD). These spectroscopic techniques have been used for various systems, however the combination with very strong magnetic field has been absent. To open this frontier, we have developed a small pulsed-magnet system for X-ray experiments.

Figure 1 shows the mini magnet used for XAS experiment up to 50 T. Thanks to the extremely small size, the magnet and the capacitor bank are portable and thus the combination with various types of X-ray spectrometer becomes possible. In fact, the capacitor bank is as small as a small refrigerator and the storing energy is only 2 kJ. Even such small system, a high magnetic field up to 50 T can be achieved. One of advantages of the system is that the magnet can be easily installed into a small space of the existing spectrometer and the cryostat system without major change.

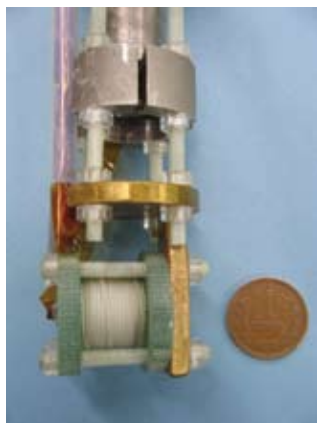


Fig. 1 A small pulsed magnet for XAS experiment. A magnetic field as high as 50 T can be generated.

The first experiment was made for the YbInCu₄, which shows a valence state transition. Namely, the magnetic moments disappear at low temperature with a first order like change of lattice volume and the non-magnetic valence fluctuation state is realized. When a magnetic field is applied, the metamagnetic like transition is observed. It has been considered as the recovery of magnetic state associated with the valence state transition. Since the transition field is above 30 T, no direct evidence of the valence change has been presented so far.

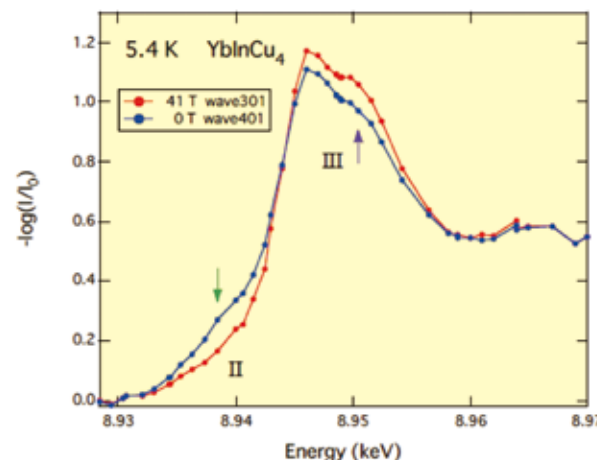


Fig. 2 XAS spectra of YbInCu₄ at 5.4 K. Yb²⁺ and Yb³⁺ components are indicated by arrows with II and III, respectively.

Figure 2 shows the XAS spectra of YbInCu₄ at 0 and 41 T. The latter is taken above the field induced valence state transition. A distinct change of spectra is observed. Namely, the Yb²⁺ component decreases at high magnetic field and, alternatively, the Yb³⁺ component increases. By fitting the spectra by a standard method, the field variation of valence of Yb ion is evaluated. Such direct determination of valence state is very unique for material investigation. It will be useful for the study of spin dependence of electronic state in many other systems.

More recently, the technique has been applied for X-ray MCD measurement of antiferromagnets. As is well known, MCD is a unique element selective method to determine spin and orbital moments. It can be applied only for ferromagnet and this limits the range of application. By using the present high magnetic field, MCD can be measured many of antiferromagnets. It would open the new field for X-ray spectroscopy.

References

- [1] Y. H. Matsuda, T. Inami, K. Ohwada, Y. Murata, H. Nojiri, Y. Murakami, H. Ohta, W. Zhang and K. Yoshimura, J. Phys. Soc. Jpn. **76**, 034702 (2007).

Contact to

Hiroyuki Nojiri (Magnetism Division)

e-mail: nojiri@imr.tohoku.ac.jp

Scanning Tunneling Microscopy/Spectroscopy Studies of Superconducting Boron-doped Diamond Films

Scanning tunneling microscopy/spectroscopy experiments have been performed on (111)-oriented epitaxial films of heavily boron-doped diamond at $T = 0.47$ K. The tunneling spectra show superconducting property and the obtained gap ratio $2\Delta/k_B T_c = 3.57$ is consistent with the weak-coupling BCS theory.

Recently, Ekimov et al. discovered superconductivity in the heavily boron-doped diamond. The superconducting transition temperature T_c was 2.3 ~ 4 K for their polycrystalline bulk samples with the boron concentration $n \sim 4.9 \times 10^{21} \text{ cm}^{-3}$. As pointed out by Takano et al., the value of T_c depends on the concentration of boron, the synthesized process, and the orientation of the film growth; thus it is interesting to study the relationship between the surface structure and superconducting property.

In order to understand the electronic state of the superconductivity in boron-doped diamond, we have performed low temperature scanning tunneling microscopy/spectroscopy (STM/STS) experiments on heavily boron-doped diamond films at $T = 0.47$ K under the ultra-high vacuum condition by using ^3He -refrigerator based STM [1]. Heavily boron-doped epitaxial diamond films ($T_c = 5.4$ K) were grown on the (111)-oriented type Ib diamond substrates by using the microwave plasma-assisted chemical vapor deposition (MPCVD) method.

The STM topography on the (111)-oriented film surface shows a regular atomic arrangement with a sixfold symmetry as shown in Fig. 1(a). The distance between nearest neighbor atoms is estimated to be ~ 0.25 nm and the value agrees with the distance between the two carbon atoms of the diamond (111) ideal surface. Since the density of the atomic hydrogen is high in the MPCVD process, the monohydride structure, $\text{C}(111)1 \times 1:\text{H}$, is most likely the structure in Fig. 1(a). This atomic structure is realized when each dangling bond of diamond (111) 1×1 is terminated by one hydrogen atom, as shown in the structure model of Fig. 1(b). The broad change of the background electronic state in Fig. 1(a) may result from the random distribution of the doped boron atom with a concentration of $\sim 3\%$.

Figure 2 shows a typical tunneling conductance spectrum dI/dV (solid circles). The tunneling spectra show the superconducting energy gap 2Δ and the coherence peak. Using the modified BCS expression for the density of states (i.e., Dynes function), $N(E, \Gamma) \propto \text{Re}(E - i\Gamma) / \{(E - i\Gamma)^2 - \Delta^2\}^{1/2}$, parameters $\Delta = 0.83$ meV and $\Gamma = 0.41$ meV are obtained from the best fit to the experimental data (see solid line). Here, Γ is the pair-breaking parameter. The gap ratio is obtained to be $2\Delta/k_B T_c = 3.57$ and the value is consistent with the theoretical value ($2\Delta/k_B T_c = 3.53$) for the weak coupling BCS superconductor. The dI/dV spectra observed in this study show the broad coherence peak, the high zero bias conductance and the relatively large value of Γ . Since these characteristic features become remarkable with increasing boron concentration, the introduced disorder by the boron doping works as the pair breaking creates which enhance the zero bias conductance.

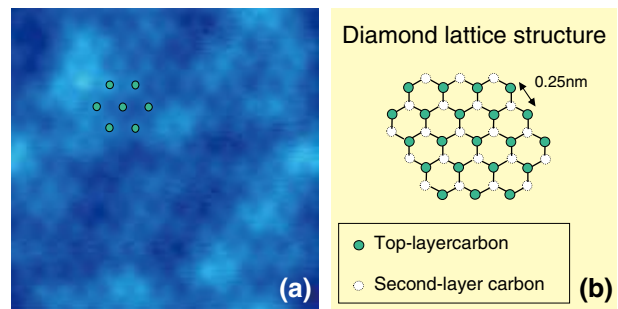


Fig.1 (a) STM topographic image of the (111)-oriented epitaxial film of heavily boron-doped diamond. ($3.2 \times 3.3 \text{ nm}^2$, $V = 500 \text{ mV}$, $I = 0.1 \text{ nA}$). (b) Structure of $\text{C}(111)1 \times 1:\text{H}$ surface.

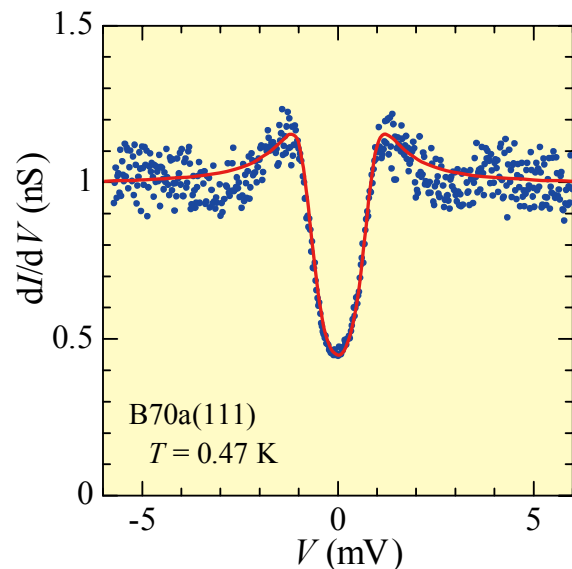


Fig. 2 Typical dI/dV spectrum (solid circles) at $T = 0.47$ K. The solid line shows a modified BCS density of states.

References

[1] T. Nishizaki, Y. Takano, M. Nagao, T. Takenouchi, H. Kawarada, and N. Kobayashi, *Science and Technology of Advanced Materials* **7**, S22 (2006).

Contact to

Terukazu Nishizaki (Low Temperature Physics Division)
e-mail: terukazu@imr.tohoku.ac.jp

Synthesis and Electronic Phase Diagram of Li_xZrNCl Superconductor

Single phase samples of Li_xZrNCl with controlled doping levels have been successfully synthesized for the first time, and an electronic phase diagram as a function of carrier concentration has been established. It has been found that T_c increases rapidly as the carrier concentration is reduced, and takes a maximum value on the verge of superconductor-Anderson-insulator transition point.

$\beta\text{-ZrNCl}$ and $\beta\text{-HfNCl}$ are band insulators with a layered structure as depicted in Fig.1, and have been known to become superconductors when doped with electrons by means of alkali-metal intercalation. According to recent band calculations, doped electrons are accommodated into ZrN or HfN double-honeycomb layers, and form a rather simple, two-dimensional electronic state. The superconducting transition temperature T_c is about 13 K and 25.5 K for Zr- and Hf-based materials, respectively. One of the most unique features of these materials is that the density of states at the Fermi level and the electron-phonon coupling constant are both very small for their T_c values, as clearly evidenced by a specific heat measurement [1]. Despite such interesting features and the relatively high T_c values, systematic investigations on the fundamental properties of these materials have thus far been prevented by the difficulties in synthesizing single phase materials and in treating the samples that are extremely sensitive to the air. We have successfully developed a method to obtain single phase samples of Li_xZrNCl with controlled doping levels, and clarified the electronic phase diagram as well as doping-evolution of physical properties of the materials [2,3].

The as-intercalated samples of Li_xZrNCl in the lightly doped region of $x < 0.1$ tend to be easily phase-separated into Li-doped and pristine phases, but we found that single phase samples can be obtained by high temperature annealing at 873 K. For thus obtained samples, we carefully confirmed the continuous and steady Li intercalation, namely the formation of solid solution, by means of synchrotron X-ray diffraction measurements at BL02B2, SPring-8 and Raman scattering technique. It should be noted that such solid solution behavior is very rare from a view point of materials chemistry of intercalation compounds. Figure 2 shows the electronic phase diagram of this system as a function of carrier concentration [2]. As the doping level is reduced from $x=0.4$, the T_c value remains almost constant, but rapidly increases below $x=0.12$, taking a maximum value of 15.2 K at $x=0.06$. At $x=0.05$, the superconducting transition suddenly disappears and the material turns to an Anderson insulator. Such an increase in T_c on the verge of the Anderson transition is quite anomalous as the T_c is gradually reduced and eventually disappears at the transition point in the case of usual superconductor-Anderson-insulator transition.

In order to see whether the observed increase in T_c can be accounted for in terms of increased electron-phonon interaction, we have performed low-temperature Raman scattering experiments for several samples with a wide doping concentration x [3]. A detailed analysis of the doping- and temperature-dependent phonon line width indicated that the electron-phonon coupling constant rather decreases as the doping concentration is reduced and the Anderson insulator is approached from the superconducting side. Therefore, it should be necessary to take some other ingredients into account to explain the observed increase in T_c on the verge of superconductor-insulator transition.

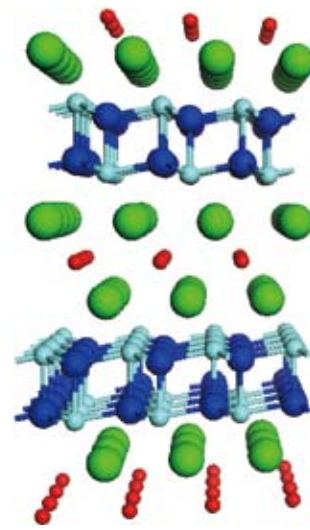


Fig.1 A crystal structure of Li_xZrNCl is schematically shown. Red, light blue, blue, and green spheres represent Li, Zr, N, and Cl atoms, respectively.

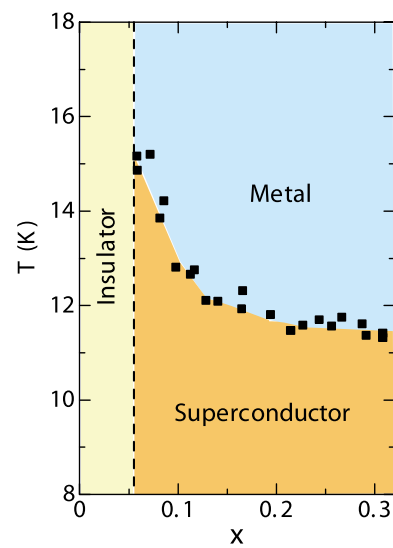


Fig.2 An electronic phase diagram of Li_xZrNCl system is shown as a function of carrier concentration.

References

- [1] Y. Taguchi, M. Hisakabe and Y. Iwasa, Phys. Rev. Lett. **94**, 21700 (2005).
- [2] Y. Taguchi, A. Kitora and Y. Iwasa, Phys. Rev. Lett. **97**, 107001 (2006).
- [3] A. Kitora, Y. Taguchi, and Y. Iwasa J. Phys. Soc. Jpn. **76**, 023706 (2007).

Contact to

Yoshihiro Iwasa (Low Temperature Condensed State Physics Division)

e-mail: iwasa@imr.tohoku.ac.jp

Anomalous Lattice Softening in Cu-oxide Superconductors Discovered by a Complementary Use of Quantum Beams of Neutron and Synchrotron X-ray

Lattice vibrations of Cu oxide superconductors with a high transition temperature (high- T_c) have been systematically studied by using both neutron and X-ray scattering. We newly discovered an anomalous softening in the Cu-O parallel bond-stretching mode which occurs in the superconducting phase of the Cu-oxide system. This observation has triggered a new direction of research on the mechanism of high- T_c superconductors.

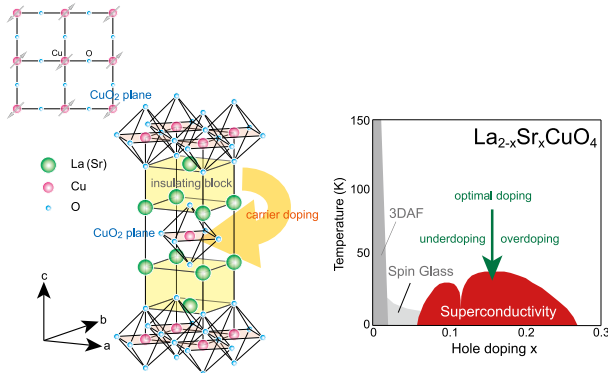


Fig. 1: Crystal structure (left) and phase diagram (right) of Sr-doped La_2CuO_4 . Superconductivity appears upon hole doping with $0.06 < x < 0.27$.

Twenty years have passed since the discovery of the first superconducting Cu-oxide, but no one can answer to a simple question why superconductivity can survive at such high temperatures beyond the boiling temperature of liquid nitrogen. Figure 1 shows the crystal structure and phase diagram of Sr-doped La_2CuO_4 (LSCO) which is one of the typical superconducting Cu-oxides. Superconductivity appears when charge carriers are doped into insulating La_2CuO_4 with substitution of La sites by Sr ions.

There have been two main streams of research on the mechanism of high- T_c superconductivity. One is the research on magnetic properties of Cu-oxides which focuses on the facts that 1) the insulating mother compounds before carrier-doping show a strong magnetic interaction between the neighboring Cu spins, and 2) well-defined dynamical spin fluctuations exist even in the superconducting phase.

The other stream is the research on the collective lattice vibrations or phonons, particularly the phonons related with the Cu-O bonding which are expected to strongly couple with doped carriers. Before the present study it is well-known that almost all the transition metal oxides commonly exhibit a softening upon carrier-doping irrespective of the existence of superconductivity. The specific phonon mode which shows the softening is a Cu-O bond-stretching wave which propagates in the direction parallel to the Cu-O bonding (parallel bond-stretching mode). We studied this mode very carefully by using both neutron and X-ray beams.

For this study we grew many large single crystals of LSCO with different Sr concentrations. Particularly, in the X-ray experiment we utilized a quasi-single crystals with a controlled gradient of Sr concentration. Since the beam spot size is of the order of 0.1mm, we can effectively study the

doping dependence by only changing the position of incoming X-ray beam spot onto the quasi-single crystals.

As shown in Fig.2, we newly found two anomalous aspects of the softening, first we found a specific doping dependence and second a softening at a specific wave number (see the figure caption for detail). Such anomalous softening strongly suggests the coupling between the specific phonons and the doped carriers. Particularly, the specific wave number corresponds to that we observed in the spin density modulation commonly seen in the superconducting phase.

Our recent study on the lattice dynamics has triggered studies which focus on the interplay between spin and lattice in this system. In near future, we can study charge response of this system directly by using X-ray inelastic scattering and can discuss interplay between spin, lattice and charge fluctuations in such strongly correlated system.

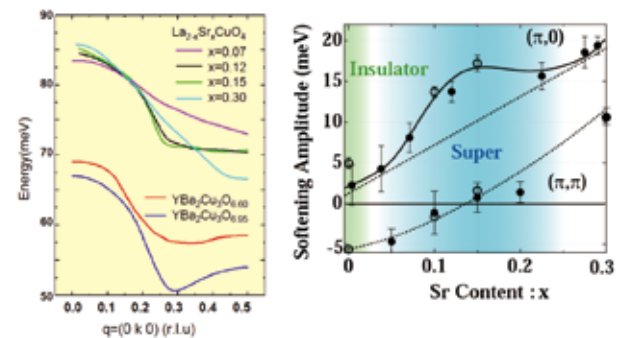


Fig.2: Dispersion curves of the Cu-O parallel bond-stretching mode for LSCO with different Sr concentrations (pink, blue, green and black lines in the left figure) and $\text{YBa}_2\text{Cu}_3\text{O}_{6+y}$ (red and purple lines in the left). All the compounds exhibit a softening of the phonon mode, but the shape of the dispersion curve, particularly the shape near the wave vector $q=0.25\sim 0.30$ depends on the compounds. Amplitude of the phonon softening (difference in the phonon frequencies between the frequencies with the wave number $q=0$ and $q=0.5$) as a function of Sr concentration (right). Only parallel bond-stretching mode (labeled by $(\pi,0)$) shows an extra softening in the superconducting concentration region. Another bond-stretching mode (labeled by (π,π)), which propagates in the direction diagonal to the Cu-O bonding, does not show such extra softening.

References

- [1] D. Reznik, L. Pintschovius, M. Ito, S. Iikubo, M. Sato, H. Goka, M. Fujita, K. Yamada, G.D. Gu and J.M. Tranquada, *Nature* **440** 1170 (2006).
- [2] K. Ikeuchi, T. Chuurei, K. Izawa, K. Yamada, Tatsuo Fukuda, Jun-ichiro Mizuki, A.Q.R. Baron, and S. Tsutsui, *J. Appl. Phys.* **45**, 1594 (2006).

Contact to

Kazuyoshi Yamada (Metal Physics with Quantum Beam Spectroscopy Division)
e-mail: kyamada@imr.tohoku.ac.jp

Dislocations in GaN: Elucidation of Dynamics and Luminescence

Defects cause spatial variations in electrical and optical functions and also their degradation of semiconductor devices. Thus, a great deal of efforts is being made in elucidating defect properties in order to control them for achieving ultimate efficiency of devices.

Gallium-nitride (GaN) is one of the most attractive semiconductors for future opto- and electronic devices as high-power/high frequency devices, blue and UV light-emitting devices, photo-detectors, chemically stable substrate, and so forth. Since dislocations are induced during hetero-epitaxial growth with a foreign substrate, fundamental knowledge on kinetics and properties of defects is crucial for addressing their stable and efficient functionalities. Key topics that should be clarified on GaN are: 1) how easily or hardly are dislocations activated into GaN and 2) what are the intrinsic opto-electric properties of dislocations? For example, there remains a controversy whether broad luminescence at around 2.2 eV, termed the yellow-band (YB), originates from recombination at dislocations generated during crystal growth. Generally, grown-in dislocations become contaminated with native point defects or impurities during the growth process. Hence, it is necessary to investigate the intrinsic properties of fresh dislocations. In these viewpoints, GaN single crystals were plastically deformed at elevated temperatures and induced fresh dislocations were evaluated in photoluminescence studies.

High quality GaN bulk single crystals can be compressively deformed at temperatures higher than 900°C. Figure 1 shows the yield stress of various semiconductors plotted against reciprocal temperature for deformation. The yield stress of GaN is around 100–200 MPa, even at 1000°C, more than two orders of magnitude higher than that of Si, Ge, GaAs, and the other compound semiconductors, and is slightly higher than that of SiC with basal slip. These results indicate that dislocations are hard to move in GaN. Thus, it is clarified that the main origin of dislocations is the lattice-mismatch with foreign substrate during epitaxial growth. From the

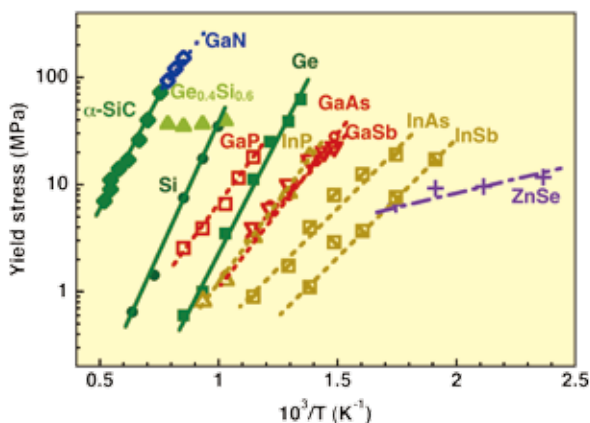


Fig. 1 Yield stresses of various semiconductors plotted against reciprocal temperature for deformation under a strain rate of $2 \times 10^{-4} \text{ s}^{-1}$.

temperature dependence of the yield stress an activation energy for dislocation motion in the GaN is estimated to be 2–2.7 eV.

By the plastic deformation a high density of fresh edge dislocations with a Burgers vector $(a/3)[11\bar{2}0]$ on the $(1\bar{1}00)$ prismatic plane are found selectively introduced into GaN. Figure 2 shows the PL spectra of a GaN crystal deformed at 950°C and a GaN crystal subsequently annealed at 950°C after deformation together with that of an as-grown GaN crystal. It is found that plastic deformation effectively leads to numerous non-radiative recombination centers that drastically reduce both near-band edge and yellow-band luminescence. That is, plastic deformation is quite effective in carrier passivation. Indeed, The deformed GaN crystals lose transparency. Fresh dislocations lead to the development of several luminescence bands centered at 1.79, 1.92, and 2.4 eV in the deep center region due to the introduction of radiative recombination centers. From the PL features dependent on deformation and annealing, it is clarified that fresh dislocations do not directly contribute to the yellow luminescence. The yellow luminescence is destroyed during the plastic deformation and recovered by subsequent annealing, which may suggest the development of a Ga vacancy-oxygen complex ($V_{\text{Ga}}\text{-O}_{\text{N}}$) due to the segregation/reaction of O impurities with dislocations being induced during the process of deformation.

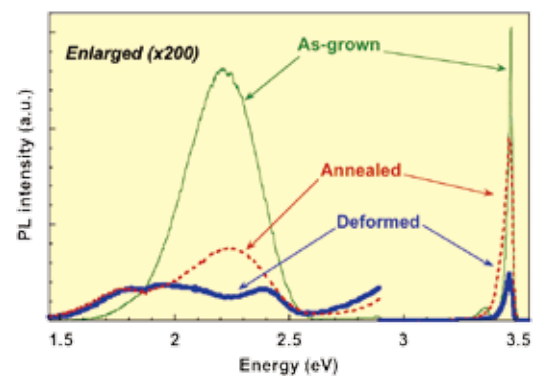


Fig. 2 Photoluminescence spectra of as-grown GaN crystal and GaN crystal deformed to a shear strain of 30% at 950°C, and GaN crystal subsequently annealed at 950°C for 2 h, measured at 11 K. PL spectra in the 1.45- to 3.1-eV photon energy range are enlarged 200 times.

References

- [1] I. Yonenaga, H. Makino, S. Itoh, T. Goto, and T. Yao, *J. Electron. Mater.* **35**, 717 (2006).
- [2] I. Yonenaga, *Mater. Trans.* **46**, 1979 (2005).

Contact to

Ichiro Yonenaga (Physics of Crystal Defects Division)
e-mail: yonenaga@imr.tohoku.ac.jp

N-Polarity GaN on Sapphire Substrate Grown by MOVPE

GaN with N-polarity opposite to Ga-polarity used in blue LEDs was successfully grown on (0001) sapphire by metalorganic vapor-phase epitaxy (MOVPE). This GaN had a mirror-like surface, and was superior to usual Ga-polar GaN in the viewpoints of X-ray diffraction measurements and the density of threading dislocations. The p-type conduction was also realized.

The progress of nitride semiconductors has been remarkable. Blue LEDs and ultraviolet LDs have been developed. Their devices are fabricated using materials with Ga-polarity (+c polarity). Usually, GaN with Ga-polarity are grown on (0001)-plane sapphire substrates by MOVPE which is suitable for mass-production. The growth of GaN with N-polarity (-c polarity) has not been reported. It has been reported that N-polar GaN tends to be pyramidal and is said to cause the rough surface. Even if the smooth surface was obtained, p-type conduction has not been realized. We report the first success in MOVPE growth of N-polarity GaN with high quality.

GaN was grown using the two-step MOVPE growth technique with low-temperature buffer layer on a (0001) sapphire substrate. Just before growth, the surface was nitrated. This nitridation was one key point for N-polarity. The 20-nm-thick GaN-buffer-layer was grown at 550°C using triethylgallium (TEG) and ammonia. TEG is decomposed at lower temperature than trimethylgallium (TMG) and carbon was hardly incorporated into the buffer layer. The annealing at 1030°C for the crystallization of a buffer layer was proceeded. In this process, it is important to control the density of nuclei. The 1~2µm-thick GaN film was successively grown at 1020°C using TMG. In this process, it is important to promote lateral growth.

The GaN polarity, which is the main subject in this paper, was carefully investigated by the coaxial impact-collision ion spectroscopy (CAICISS) and the convergent-beam electron diffraction (CBED). The spectra of CAICISS are shown in Fig. 1. Fig. 1 shows the dependence on polar angle in the azimuth of [1100]. GaN spectra are compared with single crystal ZnO because the polarity of ZnO can be determined with chemical etching. In Fig. 1, the shape of spectra for GaN is almost the same as one for ZnO -C. Therefore, GaN can be determined to have -C polarity, that is, N-polarity. In addition, the discrimination by CBED also showed the same N-polarity as by CAICISS.

The issue of surface morphology in N-polar GaN is important, because still now the N-polar GaN film has been reported to have a rough surface with many hexagons. The GaN films grown here had mirror-like smooth surfaces to the naked eye. Their surface morphologies were precisely observed by atomic force microscopy (AFM) as shown in Fig. 2. There is no pyramid, but many parallel steps are observed. From this observation, the surface is found to be atomically smooth, although pits are also observed. This film was crystallographically evaluated using four crystal X-ray diffractometer. The full width at half maximum of the spectra in ω -2 θ and ω scans is 19 and 35 arcseconds, respectively. To our knowledge, the value in ω scan is the smallest in the reported ones. The dislocation density was

investigated by TEM. The density of dislocation in this region can be counted to be $7 \times 10^8/\text{cm}^2$. This value for GaN grown by using only a GaN buffer layer is considerably small. The photoluminescence of undoped GaN was measured at room temperature. The strong near-band edge emission is observed without the yellow-band emission. Magnesium was doped into this GaN. Mg-doped GaN was annealed at 700°C for 10 minutes in nitrogen atmosphere so as to activate magnesium by diffusing out hydrogen. The carrier density was measured by Van der Pauw's method at room temperature. The density and mobility of holes was $1 \sim 3 \times 10^{17}/\text{cm}^3$ and $3 \sim 13 \text{ cm}^2/\text{Vs}$. This density is a little smaller than the reported value of GaN with Ga-polarity, because the conditions of doping and so on have not been optimized yet.

These results shatter that the N-polar GaN grown by MOVPE has a rough surface. The success of N-polar GaN means the possibility of high quality InN, which is the hottest topic in nitride semiconductors [2] and the most difficult material in nitride semiconductor because of extremely high equilibrium vapor pressure of nitrogen. In the growth of N-polarity, a nitrogen atom is caught with three gallium atoms. Therefore, by N-polar growth, the characteristics of InN can be expected to be improved. In near future, the properties of InN, which is not clear at present, will be precisely measured. Moreover, the device design becomes flexible because we can control the direction of spontaneous polarization.

References

- [1] T. Matsuoka, T. Mitate, H. Takahata, S. Mizuno, Y. Uchiyama, A. Sasaki, M. Yoshimoto, T. Ohnishi and M. Sumiya, *phys. stat. sol. (b)* **243**, 1446 (2006).
- [2] T. Matsuoka, H. Okamoto, M. Nakao, H. Harima and E. Kurimoto, *Appl. Phys. Lett.* **81**, 1246 (2002).

Contact to

Takashi Matsuoka (Advanced Electronic Materials Research Division)

e-mail: matsuoka@imr.tohoku.ac.jp

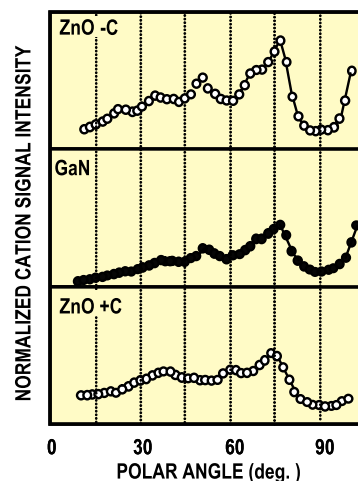


Fig. 1 CAICISS spectra of GaN and ZnO dependent on polar angle in [1100] azimuth.

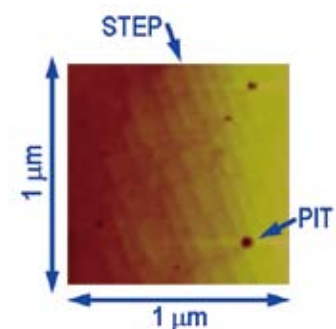


Fig. 2 AFM image.

The First Observation of Quantum Hall Effect in a Transparent Transition Metal Oxide

Transparent electronics is an emerging technology aiming at producing “invisible” electronic circuits and devices. The existence of transparent objects is not as apparent to people, so the objects can be applied in various ways in the ubiquitous network society. Such applications include security sensors, invisible electronic tags, and transparent displays. Here we have observed quantum Hall effect in a transparent oxide semiconductor, making a remark that the world’s first transparent device with a capacity close to that of a silicon semiconductor device is now realized.

Our division has been working on thin-film synthesis with various transition metal oxides and developed new devices using them. We have focused especially on ZnO, which is transparent and has electrical properties that can be varied from insulators to semiconductors and metals, also exhibiting high-efficiency ultraviolet luminescence, when optically excited. In this way, we have continued a number of attempts to improve the crystalline quality of thin-film since 1997, when we succeeded in observing ultraviolet laser emission at room temperature. In 2004, we were able to synthesize p-type ZnO for the first time in the world [1]. Meanwhile, a blue-violet light-emitting diode has been achieved.

We have recently developed technology to further enhance the quality of ZnO film, and successfully produced a device exhibiting high-electron mobility that has properties equivalent to the silicon metal-oxide-semiconductor transistor used in an integrated circuit [2]. The developed device consists of multilayers of ZnO and solid solutions of ZnO and magnesium oxide (MgZnO), with diluted two-dimensional electron gas formed between the two transparent layers (see Fig. 1). The performance of the developed device has been confirmed through the observation of the quantum Hall effect, which emerges only in exceptionally high-quality semiconductors [3].

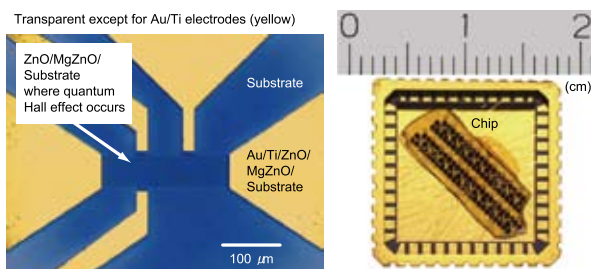


Fig. 1 Left, optical microscope image of a quantum Hall device made of ZnO; right, optical microscope image of a micropatterned Hall-bar array (film mounted on a chip carrier).

The quantum Hall effect is a well-known phenomenon for typical semiconductors such as silicon and gallium arsenide. Even though the quantum Hall effect has been applied widely as the international standard for electrical resistance, a practical application has not yet been developed. However,

the quantum Hall effect has been studied for a long time as an important research topic in the physics of condensed matter. No doubt this is because this profound physical phenomenon is of exceptional interest to researchers, in which electrical resistance coincides with the fundamental physical constant (the ratio between the charge on an electron and Planck’s constant) with a very high degree of precision, regardless of materials or nature of the elements, and it is true in our device too (see Fig. 2).

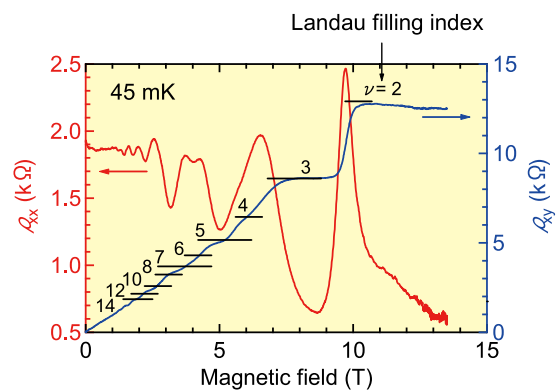


Fig. 2 Quantum Hall effect measured at 45 mK

Perhaps the significance of the experiments we have conducted lies in ushering in the field of oxide electronics, which includes transparent electronics, through the development of oxide semiconductors of practical grade. The semiconductor devices developed to date consist of semiconductors made of typical elements from the III, IV, and V families in the periodic table of elements, and many of them contain toxic elements that could pollute the environment. On the other hand, transparent semiconductors are chemically stable and biologically harmless, and are attractive materials that occur in abundant quantities in nature. Our success would facilitate further progress in the area, and there is no doubt that the history of improvement in crystal growth technology and the consequent development of high-quality devices will be repeated also with ionic crystals other than oxides and organic semiconductors.

References

- [1] A. Tsukazaki, A. Ohtomo, T. Onuma, M. Ohtani, T. Makino, M. Sumiya, K. Ohtani, S. F. Chichibu, S. Fuke, Y. Segawa, H. Ohno, H. Koinuma, and M. Kawasaki, *Nature Mater.* **4**, 42 (2005).
- [2] A. Tsukazaki, A. Ohtomo, and M. Kawasaki, *Appl. Phys. Lett.* **88**, 152106 (2006).
- [3] A. Tsukazaki, A. Ohtomo, T. Kita, Y. Ohno, H. Ohno, and M. Kawasaki, *Science* **315**, 1388 (2007).

Contact to

Akira Ohtomo (Superstructured Thin Film Chemistry Division)
e-mail: aohtomo@imr.tohoku.ac.jp

Switching of a Nanomagnet Utilizing a FePt Perpendicular Spin Injector

In the field of “Spin-electronics”, which takes advantage of the freedom of spins and provides electronic devices with multi-functionality, it has been discovered that the magnetization of a nanomagnet is switched by spin-polarized electric current, which is called current-induced magnetization reversal. This new switching technique has attracted considerable attention from fundamental and practical points of view.

When electric current flows in a magnetic nanostructure consisting of two ferromagnetic layers separated by a nonmagnetic layer, a conduction electron spin-polarized by one ferromagnetic layer (spin injector) interacts with the local magnetic moment of the other ferromagnetic layer (free layer) through the transfer of spin angular momentum. The transferred angular momentum acts as a torque to change the magnetization direction of the free layer, which is called spin-transfer torque. Thus, the magnetization direction can be manipulated without external magnetic field. Current-induced magnetization reversal is observed in current-perpendicular-to-plane giant magnetoresistance (CPP-GMR) pillars or magnetic tunnel junctions (MTJs) with the size smaller than a few hundreds nanometer, and conventional ferromagnetic materials such as Co and NiFe have usually been used for the spin injector and the free layer to date.

Our group has paid attention to L1₀-FePt alloy as a material for future spin-electronics. L1₀-FePt shows excellent thermal stability of magnetization in a nanometer scale due to the large uniaxial magnetic anisotropy (7×10^7 erg/cm³: two orders of magnitude larger than conventional ferromagnetic materials), which may lead to the large-scale integration of spin-electronic devices. In addition, the easy magnetization axis of the L1₀-FePt thin film is controlled by changing the growth condition of the thin film [1]. In other words, FePt shows either in-plane magnetization or perpendicular magnetization, which enables us to demonstrate the current-induced magnetization reversal in a variety of magnetization configurations [2,3].

Nanometer-sized CPP-GMR pillars with FePt layers are schematically illustrated in Fig. 1. One is a “conventional configuration” with only in-plane magnetized layers, and the other one is a “90° configuration” consisting of two in-plane magnetized layers and one perpendicularly magnetized layer, where the free layer is the bottom (middle) FePt layer in the conventional configuration (90° configuration). Electric current flows perpendicularly to the film plane. The change of the magnetization direction of the free layer is detected

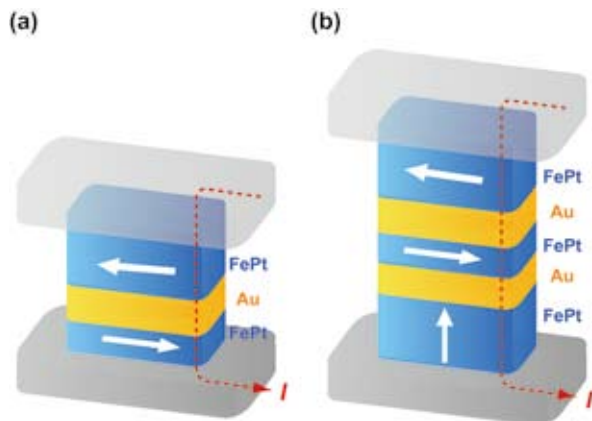


Fig. 1 Schematic illustrations of nano-sized CPP-GMR pillars for (a) a conventional configuration and (b) a 90° configuration. White arrows represent the magnetization directions. Electric current flows perpendicularly to the film plane.

as the change of device resistance (R) depending on the relative angle between two in-plane magnetized layers, which is a well-known GMR effect.

Figure 2 shows R as a function of current pulse (I_p) measured at 77K. After applying I_p , R was measured using a small sensing current. Both configurations show clear hysteretic transitions of R with sweeping I_p , where high and low resistance values correspond to the antiparallel and parallel alignments, respectively, of the two in-plane magnetized layer. These resistance changes indicate magnetization reversal is induced by electric current for both configurations. A striking feature is that the current for the magnetization reversal in the 90° configuration is obviously smaller than that in the conventional configuration. The reduction of switching current in the 90° configuration indicates that spin-transfer torque successfully acts on the magnetization of the in-plane magnetized layer from the perpendicularly magnetized layer. The FePt perpendicularly magnetized layer serves as a perpendicular spin injector to reduce the current density for magnetization reversal [2], which is an important finding for practical applications such as magnetoresistive random access memory (MRAM) requiring the low switching current. Our group also demonstrated the current-induced magnetization reversal in a perpendicular configuration, where both free layer and injector show perpendicular magnetization [3]. This perpendicular configuration has attracted much attention because of the high thermal stability of magnetization and the low switching current due to the negative shape anisotropy.

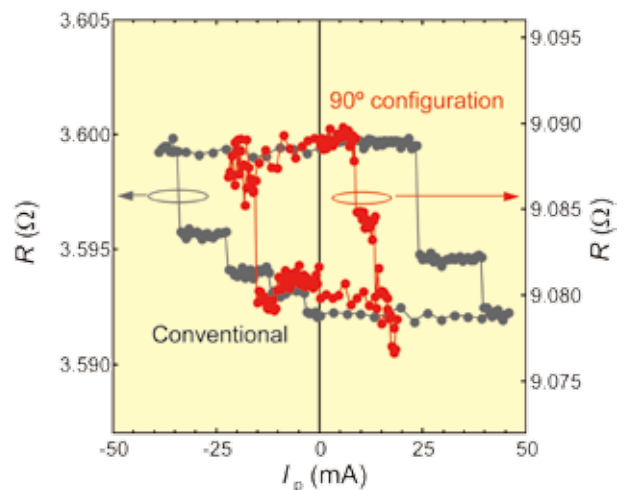


Fig. 2 Resistance R versus the amplitude of current pulse I_p for the conventional configuration (black marks) and the 90° configuration (red marks). The measurement temperature is 77K.

References

- [1] T. Seki, T. Shima, K. Takanashi, Y. Takahashi, E. Matsubara, and K. Hono, IEEE Trans. Magn. **40**, 2522 (2004).
- [2] T. Seki, S. Mitani, K. Yakushiji, and K. Takanashi, Appl. Phys. Lett. **89**, 172504 (2006).
- [3] T. Seki, S. Mitani, K. Yakushiji, and K. Takanashi, Appl. Phys. Lett. **88**, 172504 (2006).

Contact to

Koki Takanashi (Magnetic Materials Division)
e-mail: koki@imr.tohoku.ac.jp

First Heavy-fermion Superconductivity in the Neptunium Compound

Heavy fermion superconductivity is one of the most interesting topics in the condensed matter physics. In the past, several rare earth and uranium compounds were found to become superconductivity. Recently we found the neptunium based heavy fermion superconductor for the first time.

The elements, which is located at the neighbor of uranium element on the right in the periodic table, are called transuranium elements, such as neptunium, plutonium. These compounds attract much attention not only for the nuclear fuel but also for the condensed matter physics, although there are not many institutes which can treat transuranium compounds in the world, because of the strong radioactivity.

In general it is believed that neptunium compounds have 5f-itinerant features like uranium compounds. Our recent studies on de Haas-van Alphen (dHvA) experiments in NpGe₃, NpIn₃, NpNiGa₅, NpCoGa₅ and NpRhGa₅ clearly demonstrate that their Fermi surfaces can be well explained by the band calculation based on the 5f-itinerant band model[1,2]. On the other hand, the complicated magnetic properties are explained by the 5f-localized model including the orbital degree of freedom. The dual nature of 5f-electron is one of the characteristic feature in the neptunium compounds.

Recently we succeeded in growing a new neptunium compound NpPd₅Al₂ with the tetragonal crystal structure. Surprisingly, NpPd₅Al₂ is found to be the first heavy fermion superconductor in the neptunium compounds[3]. Figure 1 shows the photograph of the single crystal NpPd₅Al₂ and the crystal structure. It is characteristic that the c-value of lattice parameter is extremely larger than the a-value, meaning that the Brillouin zone becomes flat along the [001] direction.

Figure 2(a) shows the temperature dependence of the electronic specific heat in the form of C/T. The superconducting transition occurs at T_c=5K, which is relatively high compared to the other heavy fermion superconductors. The large specific heat jump of $\Delta C/\gamma T_c$ is much larger than the weak-coupling BCS value, indicating that NpPd₅Al₂ is a strong-coupling superconductor. The specific heat C at low temperatures approximately follows the T³ dependence. This indicates that the existence of anisotropic superconducting gap with point nodes.

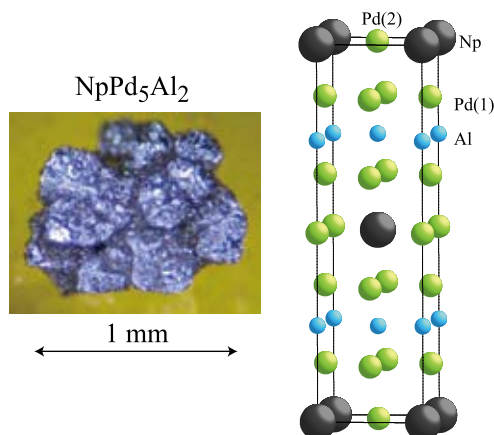


Fig. 1 (a) Photograph of NpPd₅Al₂ single crystal and (b) its crystal structure.

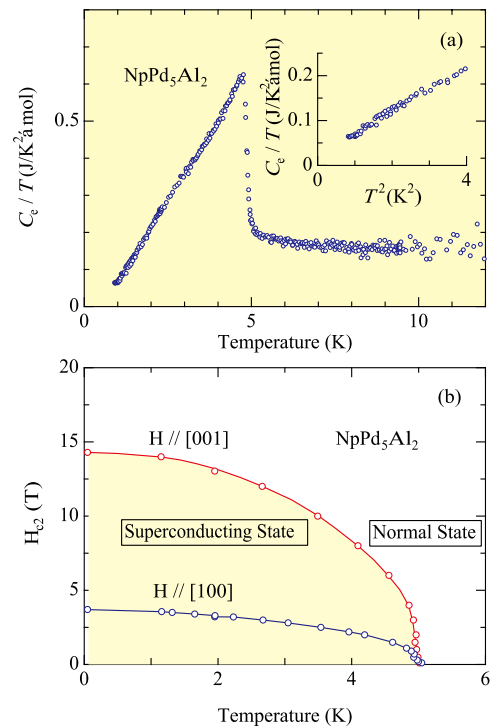


Fig. 2 (a) Temperature dependence of the electronic specific heat in NpPd₅Al₂. The large jump at 5K corresponds to the superconducting transition. (b) The temperature dependence of the upper critical field H_{c2} for H // [100] and [001].

Figure 2(b) shows the temperature dependence of the upper critical field H_{c2}, where the superconductivity is destroyed under magnetic fields. The initial slope at T_c=5K is very large for both field directions, indicating that the superconductivity is governed by the heavy quasi-particles. That is, the 5f electron with heavy effective mass becomes itinerant and contributes to the conductivity. The upper critical field is strongly suppressed with decreasing temperature, suggesting the large Pauli paramagnetic effect. The d-wave superconductivity with point nodes is most likely realized in this compound.

This work has been done in collaboration with Japan Atomic Energy Agency and Osaka University.

References

- [1] D. Aoki, Y. Homma, H. Sakai, S. Ikeda, Y. Shiokawa, E. Yamamoto, A. Nakamura, Y. Haga, R. Settai and Y. Onuki, J. Phys. Soc. Jpn. **74**, 084710 (2006)
- [2] D. Aoki, H. Yamagami, Y. Homma, Y. Shiokawa, E. Yamamoto, A. Nakamura, Y. Haga, R. Settai and Y. Onuki J. Phys.: Condens. Matter **17**, L169 (2005).
- [3] D. Aoki, Y. Haga, T. D. Matsuda, N. Tateiwa, S. Ieda, Y. Homma, H. Sakai, Y. Shiokawa, E. Yamamoto, A. Nakamura, R. Settai and Y. Onuki, J. Phys. Soc. Jpn. **76**, 063701 (2007).

Contact to

Yoshiya Homma (Radiochemistry of Metals Division)
e-mail: yhomma@imr.tohoku.ac.jp

Observation of Field-Induced Reverse Transformation in Magnetic Shape Memory Alloy Ni₅₀Mn₃₆Sn₁₄

The structural and magnetic properties of ferromagnetic shape memory alloy Ni₅₀Mn₃₆Sn₁₄ were studied by magnetization and high field X-ray powder diffraction measurements. A field induced reverse martensitic transformation was observed. In addition, it found that the large magnetoresistance effect of 50% occurs accompanied by the transformation.

Ferromagnetic Heuslar alloys Ni₅₀Mn_{50-y}Sn_y (X = In, Sn, and Sb) show martensitic transformation from the cubic L2₁-type (C) structure to an orthorhombic four-layered (4O). The alloys will become to be new candidate as actuator materials controlled by magnetic field. It is very important to reveal the magnetic, structural and thermal properties in magnetic field for development of the new magnetic materials, Ni₅₀Mn_{50-y}X_y. In this study, in order to clarify the basic properties of Ni₅₀Mn₃₆Sn₁₄ in magnetic fields, we have performed magnetization and electrical resistivity measurements in fields *B* up to 17 T, and High-Field X-ray diffraction (HF-XRD) in fields up to 5 T and in the temperature ranging from 4.2 K to 320 K at the High Field Laboratory for Superconducting Materials, Institute for Materials Research, Tohoku University.

Figure 1 shows the typical results of the HF-XRD profile of Ni₅₀Mn₃₆Sn₁₄ in fields up to 5 T at 250 K (a), 240 K (b) and 220 K (c) [1]. Here, all field dependence profiles are measured after zero-field heating from 100 K. As shown in Figs. 1(a) and 1(c), the profiles do not drastically change by applying magnetic fields up to 5 T in the L2₁ and 4O structures, respectively. In contrast, we clearly see the field-induced reverse martensitic transformation from the 4O to L2₁ type structures at 240 K, as shown in Fig. 1(b). It is first time that the field-induced reverse martensitic transformation was observed by using XRD.

Figure 2 shows the magnetoresistance (ρ -*T*) in magnetic fields up to 17 T at 4.2, 150 and 220 K. In a zero field, ρ at 4.2 (4O) and 220 K (L2₁) are 320 and 180 mΩcm, respectively, and they decreases linearly with increasing magnetic field. On the other hand, we observed large negative magnetoresistance effect in Ni₅₀Mn₃₆Sn₁₄ at the vicinity of the martensitic transformation temperature. The data at 150 K are shown in Fig.2 (red) as a typical result. The change of the negative magnetoresistance is approximately 50% in magnetic fields up to 17 T. Our recent results indicate that the structural transformation and negative magnetoresistance will be controlled in a lower magnetic field.

Results of magnetization measurements show that the magnetic moment of the L2₁ phase is larger than that of the 4O phase [1,2]. The observed field-induced reverse transformation from the 4O to L2₁ phase probably occurs to decrease the magnetic energy because of the addition of the Zeeman energy.

References

[1] K. Koyama, K. Watanabe, T. Kanomata, R. Kainuma, K. Oikawa, and K. Ishida, Appl. Phys. Lett. **88**, 132505 (2006).

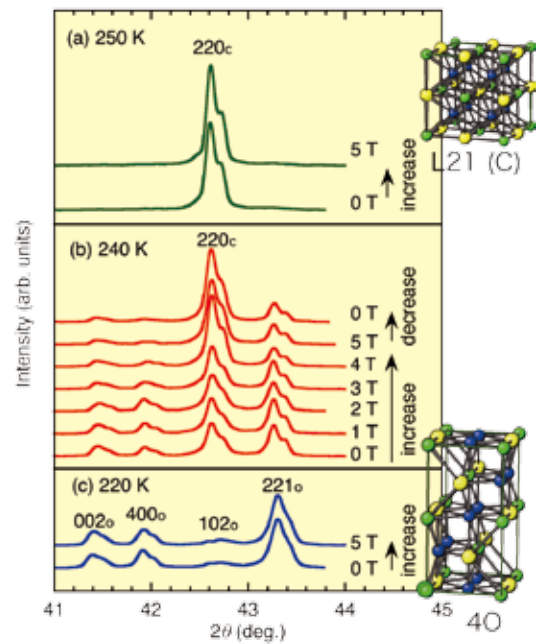


Fig. 1. XRD profiles of Ni₅₀Mn₃₆Sn₁₄ in magnetic fields up to 5 T at 250 K (a), 240 K (b) and 220 K (c). *hkl_c* and *hkl_o* denote the Miller for the cubic L2₁-type and four-layered orthorhombic (4O) structures, respectively.

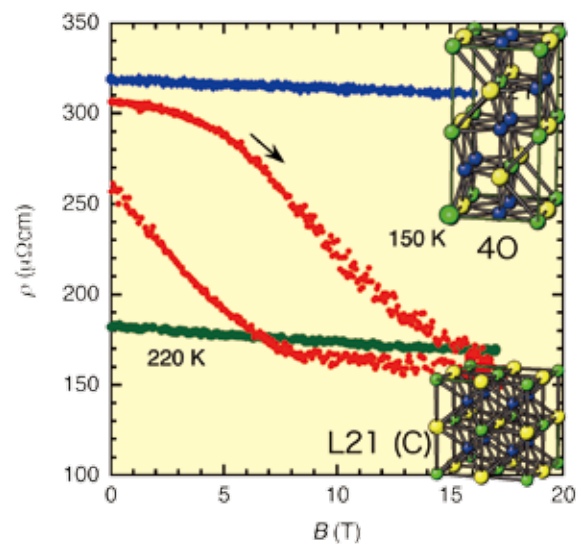


Fig.2. Magnetoresistance of Ni₅₀Mn₃₆Sn₁₄ at 4.2 K (blue), 150 K (red) and 220 K (green).

[2] K. Koyama, H. Okada, K. Watanabe, T. Kanomata, R. Kainuma, W. Ito, K. Oikawa, K. Ishida, Appl. Phys. Lett. **89**, 182510 (2006).

Contact to

Keiichi Koyama (High Field Laboratory for Superconducting Materials)

e-mail: kkoyama@imr.tohoku.ac.jp

Unusual Generation and Break Down of Massive Quasi-Particles in the Strongly Correlated Electrons System $Ce_xLa_{1-x}B_6$

We have investigated the electronic ground state in the strongly correlated electrons system $Ce_xLa_{1-x}B_6$ where local 4f electron carries plural degrees of freedom by means of the measurements of the electrical resistivity and de Haas-van Alphen effect at very low temperatures. Unusual generation and break down of the massive quasi-particles are found.

CeB_6 is well known as a typical cubic heavy fermion system. In this compound, massive quasi-particles are generated by the strong correlation between the electrons. The ground electric crystal field state of CeB_6 is the Γ_8 which carries magnetic dipole, electric quadrupole and other multipole moments.

In the diluted $Ce_xLa_{1-x}B_6$, regardless of the random distribution of magnetic Ce ions, the de Haas-van Alphen oscillations originated from massive quasi-particles are observed [1]. This indicates that periodicity of the magnetic ions is not a necessary condition of the generation of the massive quasi-particle in the system.

The quasi-particles break down with changing the Ce-concentration or magnetic field. Figure 1 displays the temperature dependence of the electrical resistivity of $Ce_xLa_{1-x}B_6$ [2]. When the Ce concentration (x) becomes low, temperature dependence of the resistivity deviates from the T^2 -law predicted by the Landau Fermi liquid theory. It shows T^D ($D < 2$) dependence in the low x region.

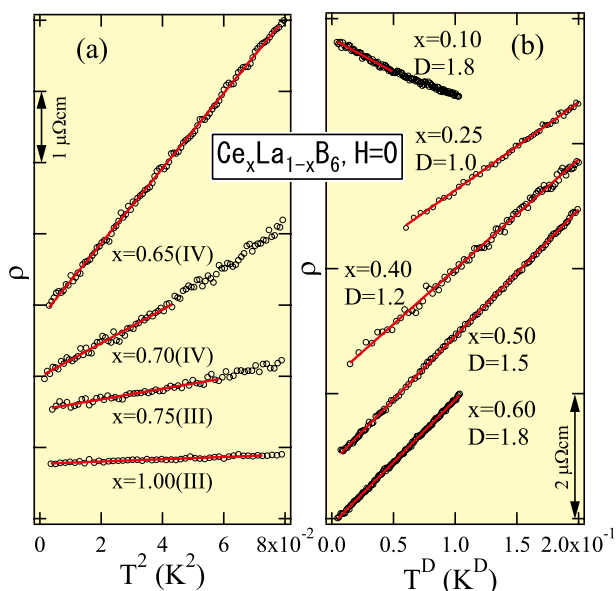


Fig. 1. (a) Temperature dependence of the electrical resistivity of $Ce_xLa_{1-x}B_6$ at zero field as a function of T^2 in the ordered phases III (antiferromagnetic state) and IV (under investigation) and (b) as a function of T^D in the paramagnetic phase (phase I) [2].

Figure 2 shows the Ce concentration and magnetic field dependence of the exponent D . Blue color indicates Fermi liquid state formed by the massive quasi-particles. Other

colors indicate non-Fermi liquid state where the massive quasi-particle picture is not applicable.

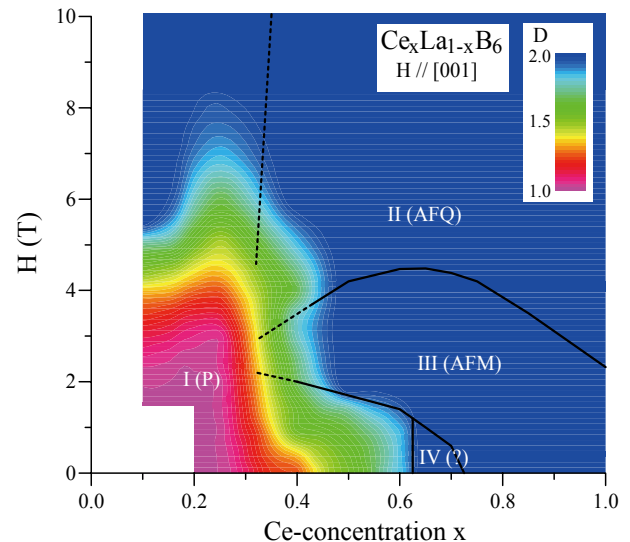


Fig. 2. Magnetic phase diagram of $Ce_xLa_{1-x}B_6$ for $H \parallel [001]$ as a function of Ce concentration (x) and field (H) at low temperatures [2]. The color denotes the value of exponent D in the temperature dependence of resistivity $\rho(T) = \rho(0) + AT^D$.

References

- [1] M. Endo, S. Nakamura, T. Isshiki, N. Kimura, T. Nojima, H. Aoki, H. Harima and S. Kunii, J. Phy. Soc. Jpn., **75**, 114704 (2006).
- [2] S. Nakamura, M. Endo, H. Yamamoto, T. Isshiki, N. Kimura, H. Aoki, T. Nojima, S. Otani and S. Kunii, Phy. Rev. Lett. **97**, 237204 (2006).

Contact to

Shintaro Nakamura (Laboratory of Low Temperature Materials Science)
e-mail: nakamura@imr.tohoku.ac.jp

First Principles Approach: Single Molecular Transistor Modulated by Transverse Field

We use a self-consistent method to study the current of the single molecular transistor modulated by the transverse field in the level of the density functional theory (DFT) and the nonequilibrium Green's function method. The numerical results show that both the polyacene-dithiol molecules and the fused-ring thiophene molecules are the potential high-frequency molecular transistors controlled by the transverse field.

Recently, the search for new active molecular devices becomes a worldwide effort as these devices represent the ultimate size limit of functional devices. The current-voltage I - V characteristics of the molecular devices show profound potential for applications, including the negative differential resistance and switches, etc. Traditionally, electronic transport phenomena are studied in the context of bulk semiconductor devices, the theoretical description of which is largely built on two premises, the effective-mass approximation and the Boltzmann transport equation. At the molecular scale, the effective-mass approximation breaks down and the electronic structure of the system must be taken explicitly into account. In a word, transport in molecular devices is different from that in semiconductor devices in two aspects, 1) the effect of the electronic structure and 2) the effect of contact.

At present, people have realized two major approaches to control quantum transport. One is through the conformational change in the molecule, and the other is through the external transverse field to switch the molecule from the "on" state to the "off" state. Now, the attention is transferred to the latter one due to its high operation frequency. The organic semiconductors can be employed as active layers in the field effect transistors FETs. At present, some theoretical works have shed light on the organic molecular transistors controlled by the transverse field. In this study, we use the self-consistent calculation of the molecular-transistor-electrode system controlled by the transverse-field effect (TFE) on the basis of DFT and nonequilibrium Green's function method.

The calculated molecular device has the sulfur atom attached by the gold electrode from both sides and the system is set under both the longitudinal and transverse fields. The potential zero point is set at the coordinate origin, the middle of the line connecting two sulfur atoms, and the whole molecule is not symmetric to the Au-S bond, which will be in favor of TFE.

Figure 2 shows the gate bias successfully controls the I - V characteristics of the pentathienoacene (PTA). At the $V_{sd} > -2.25$ V, due to the contribution from HOMO, the positive gate bias achieves the bigger molecular current and at the $V_{sd} < -2.25$ V, as LUMO enters the V_{sd} window and contributes to the molecular conduction, the inverse order of current appears. The inset illustrates the electron with spin-up number deviation from the equilibrium state as a function of V_{sd} . At $V_{sd} > -2.25$ V, for gate bias $V_g = -3.90$ V, the electron is responsible for the conduction ($N > N_0$) and electron number

rises slowly, while for $V_g > -1.95$ V, the hole is responsible for the conduction ($N < N_0$), so the electron number descends the electron flows out of the molecule to the lead. At $V_{sd} < -2.25$ V, the molecule enters the electron and hole hybrid conduction region, accompanying the rapid rise of electron number, which means that the electron contribution dominates the conduction. Both the TFE and charge effect have contributions to the I - V curves.

Moreover, our self-consistent results show that the long-length organic molecule can achieve better transport characteristics. Our investigation proves that both the polyacene-dithiol molecules and fused-ring oligothiophene molecules can be made as the high-frequency molecular transistors controlled by the transverse field.

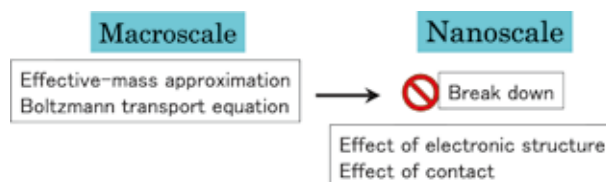


Fig. 1. Comparison between macroscale and nanoscale for conductance calculation.

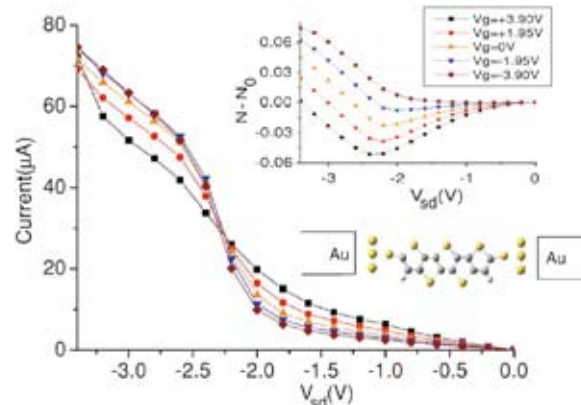


Fig. 2. Gate modulation of the I - V characteristics for PTA. The $V_{sd} = -2.25$ V is the crossover point for the current controlled by the gate bias. For $V_{sd} > -2.25$ V, either electron ($V_g = -3.90$ V) or hole ($V_g > -1.95$ V) is responsible for the current. For -3.4 V $< V_{sd} < -2.25$ V, the molecule enters the electron and hole hybrid conduction region, and the positive biased current is smaller than the negative ones.

References

F. Jiang, Y. X. Zhou, H. Chen, R. Note, H. Mizuseki, and Y. Kawazoe, *J. Chem. Phys.* 125, 084710 (2006).

Contact to

Ryunosuke Note (Center for Computational Materials Science)
e-mail: erasure@imr.edu